Proceedings of the Korean Nuclear Society Spring Meeting
Kori, Korea, May 2000

Prediction of Three-dimensional Turbulent Flow in Curved Piping Systems Susceptible to Flow-Accelerated Corrosion

Jong Chull Jo and Yun Il Kim

Korea Institute of Nuclear Safety
19 Kusung-dong, Yusung-ku, Taejon 305-338, Korea

Abstract

The three-dimensional turbulent flow in curved pipes susceptible to flow-accelerated corrosion has been analyzed numerically to predict the pressure and shear stress distributions on the inner surface of the pipes. The analysis employs the body-fitted non-orthogonal curvilinear coordinate system and a standard $k-e$ turbulence model with wall function method. The finite volume method is used to discretize the governing equations. The convection term is approximated by a high-resolution and bounded discretization scheme. The cell-centered, non-staggered grid arrangement is adopted and the resulting checkerboard pressure oscillation is prevented by the application of a modified version of momentum interpolation scheme. The SIMPLE algorithm is employed for the pressure and velocity coupling. The numerical calculations have been performed for three curved pipes with different bend angles and curvature radii, and discussions have been made on the distributions of the primary and secondary flow velocities, pressure and shear stress on the inner surface of the pipe to examine applicability of the present analysis method. As the result, it is seen that the method is effective to predict the susceptible systems or their local areas where the fluid velocity or local turbulence is so high that the structural integrity can be threatened by wall thinning degradation due to flow-accelerated corrosion.

1. Introduction

The corrosion-caused wall thinning of the pipe and vessel systems in high pressure systems at nuclear power plants can result in catastrophic failures of the systems accompanying a large amount of release of steam and water into the environment. This leakage has such serious implications as the loss of the coolant and the direct release of radioactive fission products to the plant areas occupied by personnel. The pipe failures can also damage surrounding equipment although it is not common. It has been reported that nuclear power plant availability and revenue losses attributed to corrosion is significant [1]. Thus such problems with corrosion damage to the pipe and vessel system present safety concerns and economic consequences.

The corrosion mechanisms causing the wall thinning are known to be inter-granular stress corrosion cracking (IGSCC), generalized corrosion, microbiologically-influenced corrosion (MIC), flow-accelerated corrosion (FAC), corrosion fatigue, cavitation-induced erosion, etc. Several nuclear power plants irrespective of reactor types throughout the world have been so far experiencing the FAC [1, 2]. For this reason, it has been recognized as a worldwide major issue in all types of nuclear power plants including PWRs, BWRs, CANDU, and gas-cooled reactors since around 1970. The United States Nuclear Regulatory Commission issued the Bulletin 87-1 [3] in 1987 and the Generic Letter 89-08 [4] in 1989, requiring all U.S. nuclear plants to institute long-term, comprehensive programs to prevent pipe ruptures caused by FAC.

Basically, a comprehensive evaluation program to avoid potential ruptures caused by FAC includes the activity of identifying susceptible systems to determine the scope of program. To identify the system or its local part that is expected to be susceptible to the FAC, it is required to predict or measure the velocity and temperature distributions. However the direct measurement is impractical generally. Therefore, in that case, the prediction is required as a prerequisite for determining the scope of inspection program to identify the positions of thinned wall for taking necessary measures to avoid potential ruptures.

This paper presents an effective finite volume method for calculating the three-dimensional turbulent flow in curved pipes that employs the body-fitted non-orthogonal curvilinear coordinate system and a standard

$k-e$ turbulence model with wall function method [5]. The convection term is approximated by a higher-order bounded scheme named COPLA [6], which is known as a high-resolution and bounded discretization scheme. The cell-centered, non-staggered grid arrangement is adopted and the resulting checkerboard pressure oscillation is prevented by the application of modified momentum interpolation scheme [7]. The SIMPLE algorithm [8] is employed for the pressure and velocity coupling.

For examining the applicability of the method to the prediction of the local areas inner pipe surface susceptible to wall thinning degradation due to flow-accelerated corrosion, the steady turbulent flows in three different curved pipes with their bend angles of 90°, 120° and 150° have been analyzed in this study. Detailed discussions have been made on the distributions of the primary and secondary flow velocities, pressure and shear stress on the inner surface of the pipe.

2. Mathematical formulation

Governing equations

Assuming that the fluid flowing through curved piping systems is Newtonian with constant properties, the governing equations for conservation of mass, momentum and transport in a generalized coordinate system can be written as follows:

Mass conservation equation

$$\frac{\partial}{\partial x^j}(U_j)=0 \tag{1}$$

where $U_i = r\, u_k b_k^i$

Momentum equations

$$\frac{\partial}{\partial x^j}\left[U_j u_i - \frac{(m+m_t)}{J}\left(\frac{\partial u_i}{\partial x^m}B_m^j + b_k^j w_i^k\right) + P b_i^j\right] = 0 \tag{2}$$

where $B_m^j = b_k^j b_k^m$, $w_j^i = \frac{\partial u_i}{\partial x^k} b_j^k$, $m_t = C_m r k^2 / e$

and u_k denotes the three Cartesian velocity components in the directions of the transformed coordinates $y^i = y^i(x^j)$. The geometric coefficients b_i^j represent the cofactors of $\partial y^i / \partial x^j$ in the Jacobian matrix of the coordinate transformation, J stands for the determinant of the Jacobian matrix and y^i is the Cartesian coordinate system. In the above equations r, m, m_t, p, C_m, k and e denote respectively density, viscosity, turbulent viscosity, pressure, constant, turbulence kinetic energy, and the dissipation rate of turbulence kinetic energy.

Transport equation for k

$$\frac{\partial}{\partial x^j}\left[U_j k - \frac{1}{J}\left(m + \frac{m_t}{s_k}\right)\frac{\partial k}{\partial x^m}B_m^j\right] = J\left(G - re\right) \tag{3}$$

Transport equation for e

$$\frac{\partial}{\partial x^j}\left[U_j e - \frac{1}{J}\left(m + \frac{m_t}{s_e}\right)\frac{\partial e}{\partial x^m}B_m^j\right] = J\left(C_{e_1}\frac{e}{k}G - C_{e_2}\, r\frac{e^2}{k}\right) \tag{4}$$

where, $C_{e_1} = 1.44$, $C_{e_2} = 1.92$, $C_m = 0.09$, $s_k = 1.0$, $s_e = 1.3$

In the above equations (3) and (4), G is the turbulence source term and is defined as follows:

$$G = \frac{m_t}{J^2}\left[2\left(\frac{\partial u_j}{\partial x^m}b_j^m\right)^2 + \left(\frac{\partial u_1}{\partial x^m}b_2^m + \frac{\partial u_2}{\partial x^m}b_1^m\right)^2 + \left(\frac{\partial u_1}{\partial x^m}b_3^m + \frac{\partial u_3}{\partial x^m}b_1^m\right)^2 + \left(\frac{\partial u_2}{\partial x^m}b_3^m + \frac{\partial u_3}{\partial x^m}b_2^m\right)^2\right]$$

Boundary conditions

Consider a general situation of fluid flow in a curved piping system with arbitrarily shaped boundaries where a

fluid of the specified initial temperature is flowing through the piping system at a constant flowrate so that the steady flow condition is maintained. If the solution domain is symmetrical thermally and geometrically, only half of the region is needed to analyze. Thus along the symmetry line, the symmetry boundary conditions can be applied for all velocity components. On the solid wall, the wall function method is applied. For this situation the boundary conditions are given by

$u_i = u_{i,in}$, $k = k_{in}$, $e = e_{in}$ at the pipe inlet (5a)

Wall functions at the inner surface[5] (5b)

$u_2 = 0$, $\frac{\partial u_1}{\partial x^3} = \frac{\partial u_3}{\partial x^3} = \frac{\partial k}{\partial x^3} = \frac{\partial e}{\partial x^3} = 0$ at the symmetry plane (5c)

$\frac{\partial u_1}{\partial x^2} = \frac{\partial u_2}{\partial x^2} = \frac{\partial u_3}{\partial x^2} = \frac{\partial k}{\partial x^2} = \frac{\partial e}{\partial x^2} = 0$ at the outer boundary of an infinitesimal coaxial cylinder inside the pipe (5d)

$\frac{\partial k}{\partial x^1} = \frac{\partial e}{\partial x^1} = 0$ at the pipe outlet (5e)

In addition, the velocity components are adjusted to satisfy the overall mass conservation at the outlet of the pipe.

3. Numerical method of solution

Solution domain discretization

The equations (1) – (5) are solved numerically by a finite volume approach [8], requiring the discretization of the solution domain into a finite number of hexahedral control volume cell whose faces are coincided with the non-orthogonal curvilinear coordinate lines. A typical control volume is shown in. 1. The numerical grids are generated for a half symmetric region of the domain by using an algebraic method.

Discretization of governing equation

The discretization of the governing equations is performed following the finite volume approach, and the convection terms are approximated by a higher-order bounded scheme named COPLA [6].

4. Momentum interpolation method

For the present analysis, the Rhie and Chows scheme [9] is modified to obtain a converged solution for steady flows that is independent of the relaxation factors. The momentum equations are solved implicitly at the cell-centered locations in the Rhie and Chows scheme. The discretized form of momentum equations for the cell-centered velocity components u_i can be written with the under-relaxation factors expressed explicitly as follows:

$$u_{i,P} = (H_{u_i})_P + (D^1_{u_i})_P (P_w - P_e)_P + (D^2_{u_i})_P (P_s - P_n)_P + (D^3_{u_i})_P (P_b - P_t)_P + (1-\alpha_{u_i}) u^{l-1}_{i,P} \quad (6)$$

where $H_{u_i} = \alpha_{u_i} \left\{ \sum A^{u_i}_{nb} u_{i,nb} + (S^{u_i}_c \Delta V) \right\} \Big/ A^{u_i}_P$, $D^j_{u_i} = \alpha_{u_i} b^j_i / A^{u_i}_P$, $A^{u_i}_P = \sum A^{u_i}_{nb} - S^{u_i}_P \Delta V$

and α_{u_i} $(i = 1,2,3)$ are the under-relaxation factors for the velocity components u_i and the superscripts $l-1$ denote the iteration level, respectively.

The discretized form of momentum equations for the cell face velocity component, for example at the east face, can be written as follows.

$$u_{i,e} = (H_{u_i})_e + (D^1_{u_i})_e (P_P - P_E) + (D^2_{u_i})_e (P_{se} - P_{ne}) + (D^3_{u_i})_e (P_{be} - P_{te}) + (1-\alpha_{u_i}) u^{l-1}_{i,e} \quad (7)$$

In the present modified Rhie and Chow' s scheme, this cell face (the east face) velocity component is obtained explicitly through the interpolation of momentum equations for the neighboring cell centered Cartesian velocity components. Following assumptions are introduced to evaluate these east cell face velocity components. For

example, the assumptions for evaluation of the cell face velocity component u_1 can be expressed as follows:

$$(H_{u_1})_e \approx f_e^+ (H_{u_1})_E + (1-f_e^+)(H_{u_1})_P \tag{8}$$

$$(D^2_{u_1})_e (P_{se} - P_{ne}) \approx f_e^+ (D^2_{u_1})_E (P_s - P_n)_E + (1-f_e^+)(D^2_{u_1})_P (P_s - P_n)_P \tag{9}$$

$$(D^3_{u_1})_e (P_{be} - P_{te}) \approx f_e^+ (D^3_{u_1})_E (P_b - P_t)_E + (1-f_e^+)(D^3_{u_1})_P (P_b - P_t)_P \tag{10}$$

$$\frac{1}{(A_P^{u_1})_e} \approx \frac{f_e^+}{(A_P^{u_1})_E} + \frac{(1-f_e^+)}{(A_P^{u_1})_P} \tag{11}$$

where f_e^+ is the geometric interpolation factor defined in terms of distances between nodal points. Similar assumptions can be introduced for evaluation of the velocity component at the north and top faces.

Using above assumption, the velocity component $u_{1,e}$ can be obtained as follows:

$$\begin{aligned} u_{1,e} = &\left[f_e^+ u_{1,E} + (1-f_e^+) u_{1,p} + (D^1_{u_1})_e (P_p - P_E) - f_e^+ (D^1_{u_1})_E (P_w - P_e)_E - (1-f_e^+)(D^1_{u1})_P (P_w - P_e)_P \right] \\ &+ (1-a_{u_1}) \left[u^{l-1}_{1,e} - f_e^+ u^{l-1}_{1,E} - (1-f_e^+) u^{l-1}_{1,P} \right] \end{aligned} \tag{12}$$

The term in the first bracket of right hand side of equation (12) is the original Rhie and Chow's scheme. Majumdar [10] has revealed that the converged solution is relaxation factor dependent if the term in the second bracket is omitted.

5. Results and discussions

The present numerical method has been well verified by showing the excellent agreements between the predicted results for a three-dimensional transient laminar stratified flow in a duct with the available experimental data [11].

In this study, the three-dimensional turbulent flows in the three curved pipes having their respective bend angles of 90°, 120° and 150° have been analyzed using the present solution method. The geometry with numerical grid of the pipe with α° bend is shown in Fig. 2. For the pipe, the inner diameter, lengths of the two straight parts of the pipe are $0.059\,m$, $0.17\,m$ and $0.5\,m$, respectively. The radii of intrados curvature of the bend parts for the three piping systems are $0.076\,m$, $0.0855\,m$ and $0.095\,m$, respectively. In addition, the density, viscosity, and inlet velocity of the fluid are $864.3\,kg/m^3$, $0.112\times10^{-3}\,kg/m\cdot s$, $10.1317\,m/s$, respectively. The convergence is declared when the maximum of the absolute sum of the residuals of three momentum equations, pressure correction equation and two transport equations is less than 10^{-4}.

Fig. 3 shows contours of the non-dimensional primary flow velocity, which is defined by applying the specified inlet velocity of fluid as the reference scale, at the eight selected cross-sections as indicated in Fig. 2(a) for the 90° curved pipe. As shown in Fig. 3, the primary velocity distribution at the cross section 'a' near the inlet is uniform and it becomes non-uniform as the fluid flows upward to the curved part of pipe. The local fluid velocity near the extrados of inner pipe wall increases to its maximum magnitude at the mid-positioned cross-section of the curved part, while the fluid velocity near the intrados of inner wall decreases to its minimum magnitude at the same cross-section, and then decreases beyond the curved part. This implies that the primary fluid velocity near the extrados of inner wall of the curved part is much greater than that near the intrados of inner wall.

Fig. 4 displays the development of secondary flow motion at the eight cross-sections of the 90° curved pipe. These figures show the typical development of secondary motion in a curved section of pipe by the centrifugal force. The secondary motion is developed when the fluid passes through the curved part of the pipe and diminishes in the downstream of the horizontal straight pipe part. There exists a relatively strong clockwise vortex at the outlet area of curved pipe part due to the relatively strong primary flow motion in the latter half part of the curved pipe part.

As mentioned earlier, one of the parameters governing the mass transfer of iron in the oxide into the fluid stream is the fluid velocity (or the shear stress on the wall). It was found from the experimental investigations [2] that increased velocity of the flowing fluid accelerate the rate of wall thinning by further aiding the oxide and metal dissolution. In single–phase flow at high flow velocities, erosion is the destruction of the mechanical surface of a material, and the dominant mechanisms are variations in the fluid velocity and shear stress which

comes from the force exerted on the inner wall surface of pipe by the fluid and causes pressure drop. The wall surface shear stress determines if the surface of a material will break down and be subject to wear by erosion. Therefore, it is very important to calculate with accuracy the distributions of shear stress on the inner wall surface in the FAC analysis of a piping system. In this study, the wall surface shear stress t_w for turbulent flow has been calculated using the wall function.

Figs. 5 and 6 show the circumferential distributions of the pressure coefficient C_p and the non-dimensional shear stress t_w^* on the inner wall surface at the selected eight cross-sections of each pipe, respectively. C_p and t_w^* are defined as follows:

$$C_p = (p(i,j,k) - p(1,1,1))/0.5\,r\,u_{in}^2 \quad , \qquad t_w^* = t_w/0.5\,r\,u_{in}^2 \tag{13}$$

where $t_w = \sqrt{t_{y^1}^2 + t_{y^2}^2 + t_{y^3}^2}$

The shear stress implies the gradient of fluid velocity in the direction of outward normal to the inner wall surface as can be seen easily from the definition of t_w. As shown in Figs. 5 and 6, the variations in the wall surface shear stress distributions in the circumferential direction become significant in the curved part of pipe due to acceleration and deceleration of flow by the centrifugal force. This is one reason why the extrados inner wall of curved pipe part is the most likely to be thinned due to flow accelerated corrosion.

Figs. 7(a), 7(b), and 7(c) present the non-dimensional longitudinal shear stress distributions at the inner wall of the three different curved pipes, respectively. These figures clearly show the acceleration and deceleration of velocity field near the wall in the curved section of the pipe. Thus the shear stress distributions in the curved parts of the pipes vary noticeably not only in the circumferential direction but also in the longitudinal direction.

The figures indicate that as the fluid passes through the curved part, the shear stress increases steeply to its maximum value at a location in the first half of the curved part and then decreases relatively less steeply. On the contrary, the shear stress on the intrados inner wall surface decreases steeply to its minimum value at a location in the first half of the curved part and then increases slowly. As the bend angle α of curved pipe increases, those locations where the shear stresses on the extrados and intrados of inner pipe wall surface have the maximum and minimum values, respectively, move backward to the center region of curved part. These figures also show that the shear stress at the intrados pipe wall becomes greater than that at the extrados wall in the second straight part of pipe while vice versa at the extrados wall in the first straight and curved parts of each pipe as can be expected. These phenomena can be easily understood if we consider the acceleration and deceleration of flow field by the centrifugal force when the flow passes through the curved section. It is observed in Figs. 5-7 that the shear stresses at the extrados inner wall of curved pipe with smaller bend angle are higher than those with greater bend angle, and that the magnitude of shear stress decreases as the bend angle of pipe increases.

According to the results of this study, the present numerical method is considered to be effective to predict the susceptible systems or their local areas where the fluid velocity or local turbulence is so high that the structural integrity can be threatened by wall thinning degradation due to flow accelerated corrosion.

6. Conclusions

An efficient numerical method using the finite volume approach for calculating the turbulent flow in curved pipes has been presented. The method employs the body-fitted non-orthogonal curvilinear coordinate system to accommodate the complex shape of the pipes and a standard $k-e$ turbulence model with wall function method to simulate the turbulent flow in the calculations. As an illustrative problem of turbulent flows in curved pipes, the steady turbulent flows in three different curved pipes having their respective bend angles of 90°, 120°, and 150° have been analyzed in this study. Detailed discussions have been made on the distributions of the primary and secondary flow velocities, pressure and shear stress on the inner wall surface of the pipe by explaining the reasonable physical meanings for the predicted results distinctly.

Consequently, the present numerical method is considered to be valid and effective to predict the susceptible systems or their local areas where the fluid velocity or local turbulence is so high that the structural integrity can be threatened by wall thinning degradation due to flow accelerated corrosion.

Although this paper addressed a typical case, it is emphasized that the present method can be extended for applications to various cases of turbulent stratified flows in pipes and tanks with complex geometry and different flow conditions.

References

[1] Eldridge, M., (1995), *1993 and 1994 (Through September) Losses due to Material Failure*, EPRI Report prepared by RCG/Hagler Bailly, Inc.

[2] Chexal, B., et al. (1996), *Flow-Accelerated Corrosion in power plants*, EPRI TR-106611, Electric Power Research Institute.

[3] US NRC Bulletin 87-01 (1987), Thinning of pipe walls in Nuclear Power Plants.

[4] US NRC Generic Letter 89-08 (1989), Erosion/ Corrosion-Induced Pipe Wall Thinning.

[5] Peric, M., (1985), " A Finite Volume Methods for the Prediction of Three Dimensional Fluid Flow in Complex Ducts," Ph.D. Thesis, Mech. Engineering Dept., Imperial College, London.

[6] Choi, S. K., Nam, H. Y. and Cho, M. (1995), "Evaluation of a Higher-Order Bounded Scheme: Three-Dimensional Numerical Experiments," Num. Heat Transfer, Part B, Vol.28, pp.23-28.

[7] Jo, J. C., Kim, Y. I. and Choi, S. K., "Heat Transfer Analysis of Thermal Stratification in Piping Connected to Reactor Coolant System.": in Proceedings of the 1st Korea-Japan Symposium on Nuclear Thermal Hydraulics and Safety, Paper No. WR-13, pp.191-198, 1998.

[8] Patankar, S. V. (1980), *Numerical Heat Transfer and Fluid Flow*, Hemisphere, Washington, DC.

[9] Rhie, C. M., and Chow, W. L. (1983), "Numerical Study of the Turbulent Flow Past an Airfoil with Trailing Edge Separation," AIAA J., Vol. 21, No. 11, pp. 1525-1532.

[10] Majumdar, M. (1988), "Role of Under-relaxation in Momentum Interpolation for Calculation of Flow with Non- staggered Grids," Numerical Heat Transfer, Vol. 13, pp. 125-132.

[11] Jo, J. C., and Choi, S. K. (1999), "Development of a Three-Dimensional Thermal-Hydraulic Analysis Code for Thermally Stratified Flow in a Curved Piping System," Proceedings of the Korean Nuclear Society Spring Meeting, Pohang.

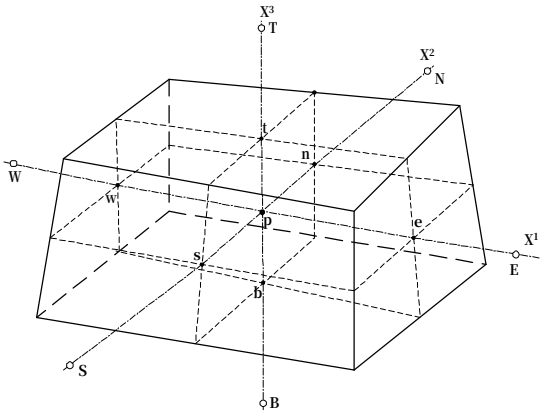

Fig. 1 Hexahedral control volume cell

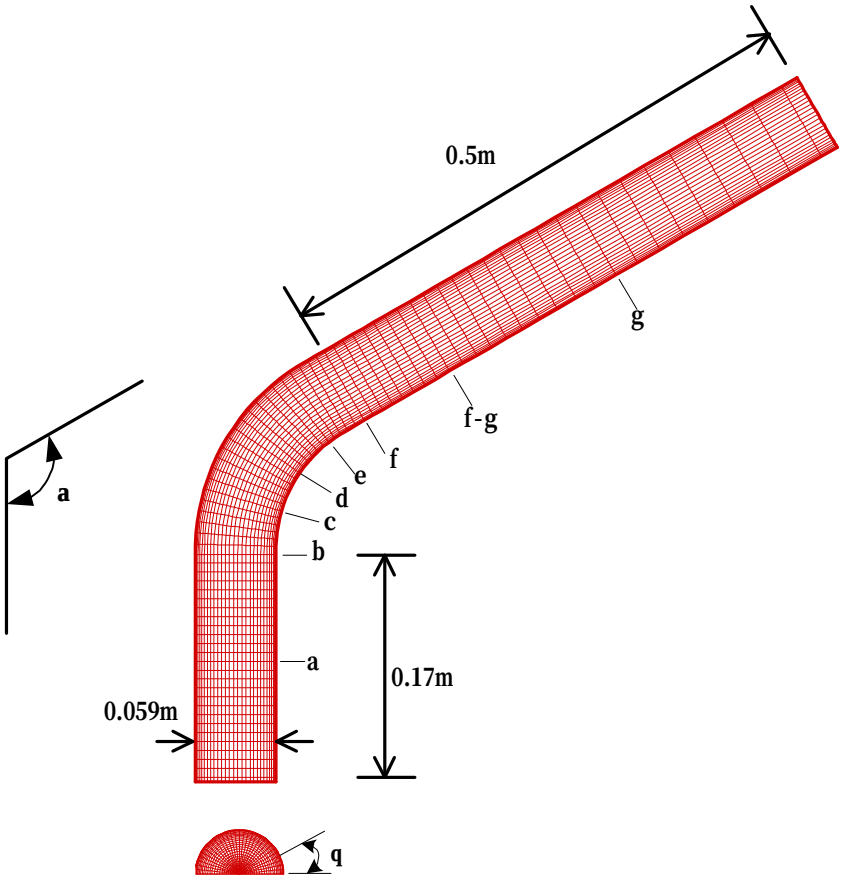

Fig. 2 Geometry and numerical grid for a curved pipe with bend angle of *a*

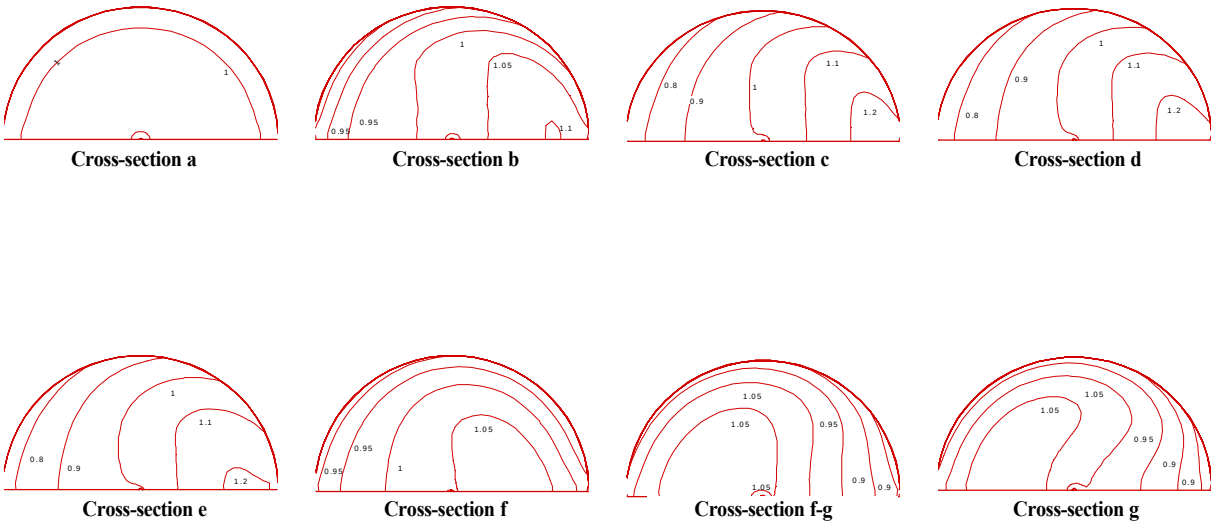

Fig. 3 Contours of the primary flow velocities parallel to the centerline of the curved pipe with α of 90°

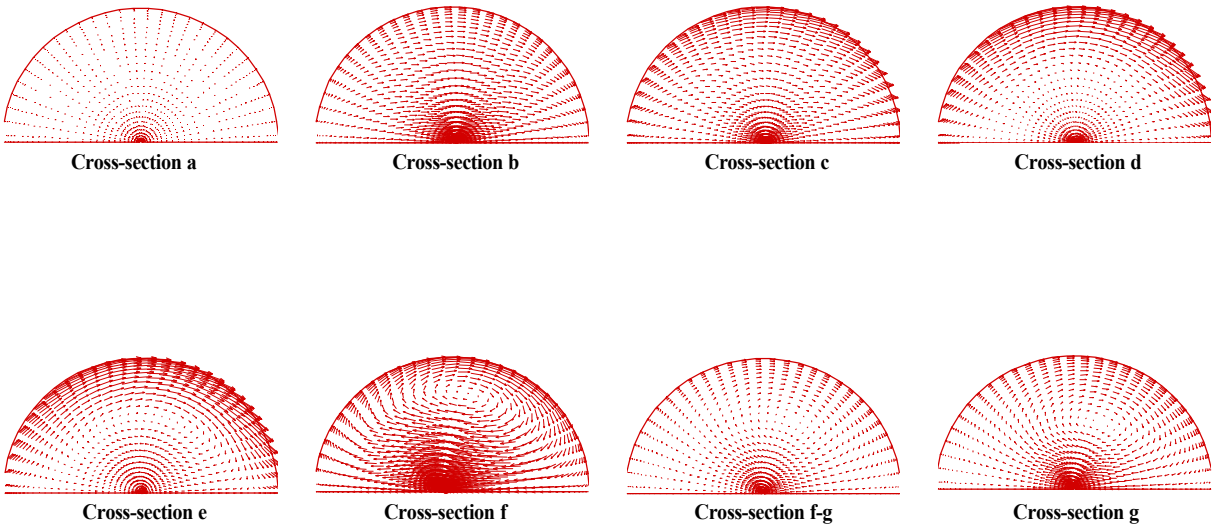

Fig. 4 Secondary flow motion in the curved pipe with α of 90°

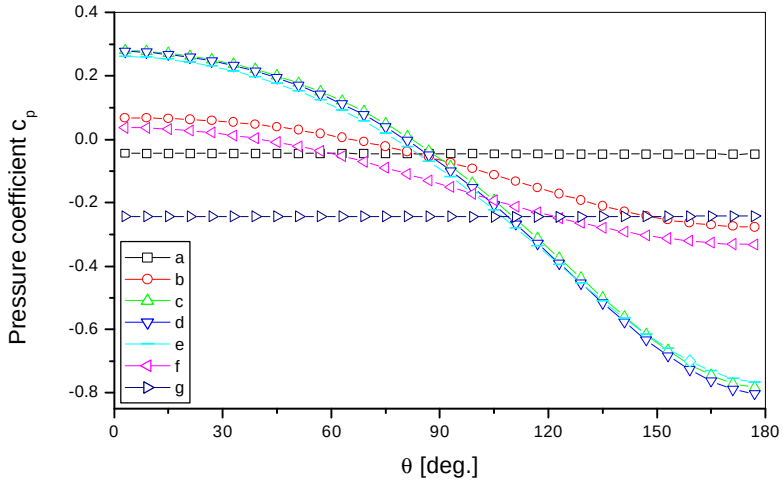

(a) α=90°

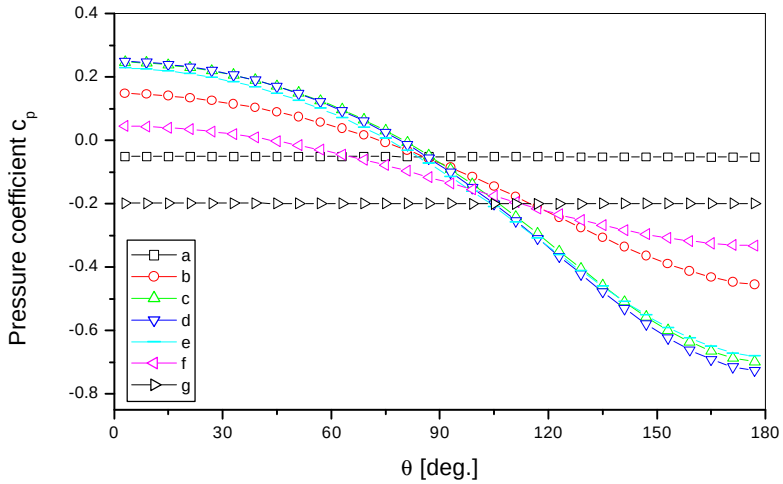

(b) α=120°

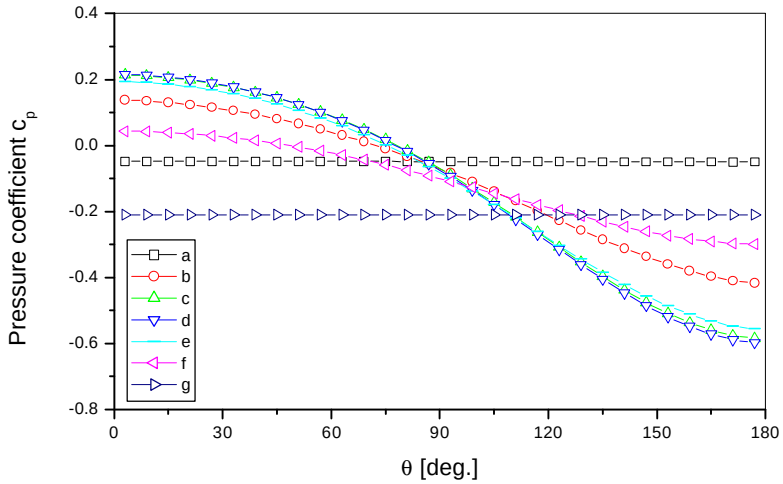

(c) α=150°

Fig. 5 Circumferential pressure coefficient distributions at the inner wall for the three curved pipes with different bend angles

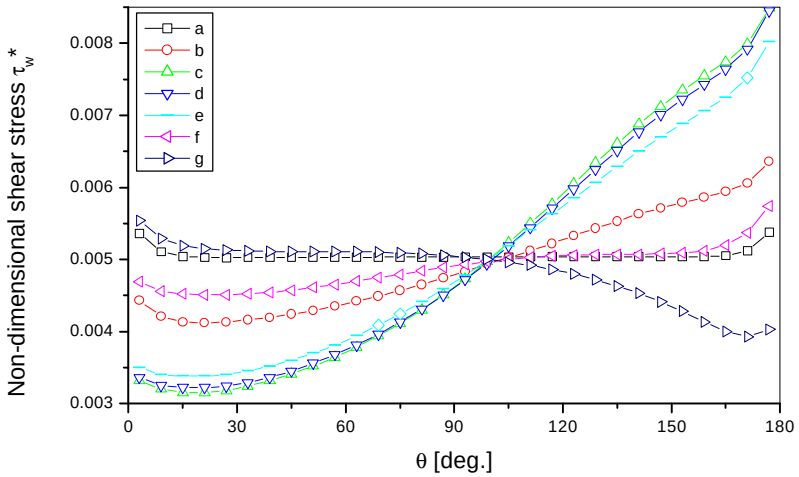

(a) α=90°

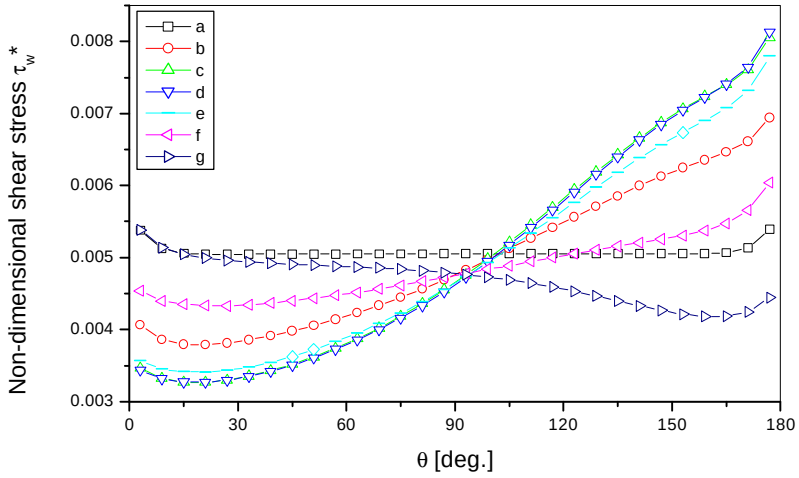

(b) α=120°

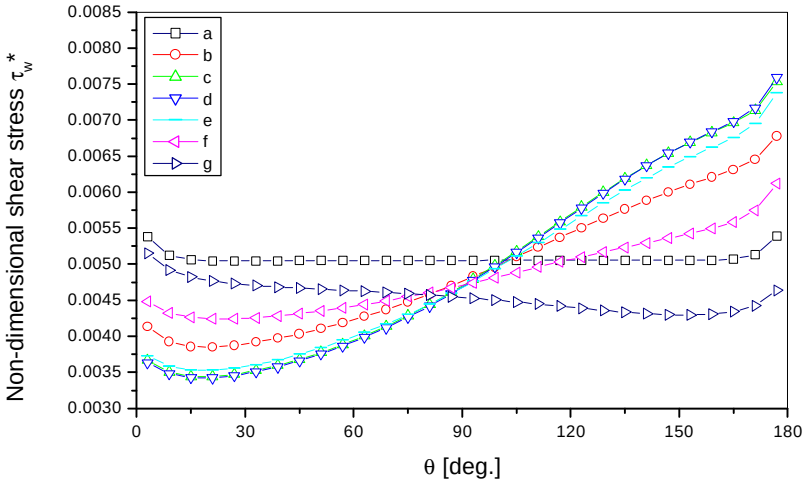

(c) α=150°

Fig. 6 Non-dimensional circumferential shear stress distributions at the inner wall for the three curved pipes

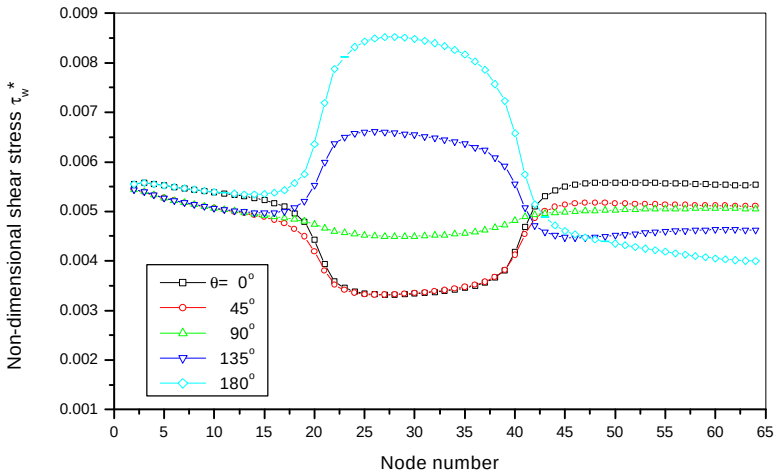

(a) α=90°

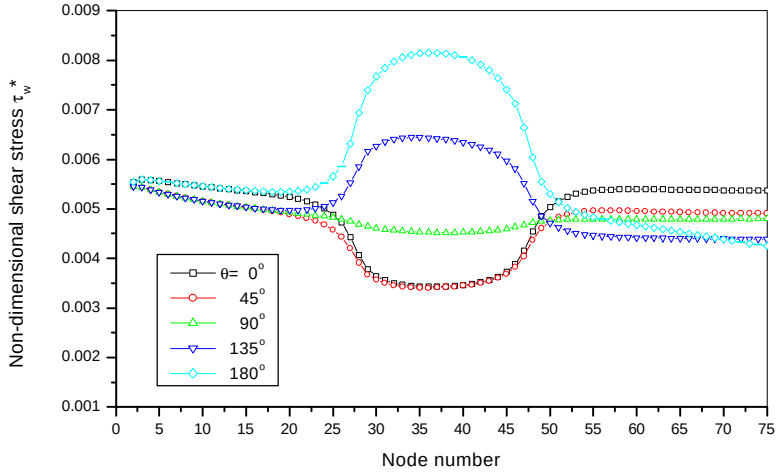

(b) α=120°

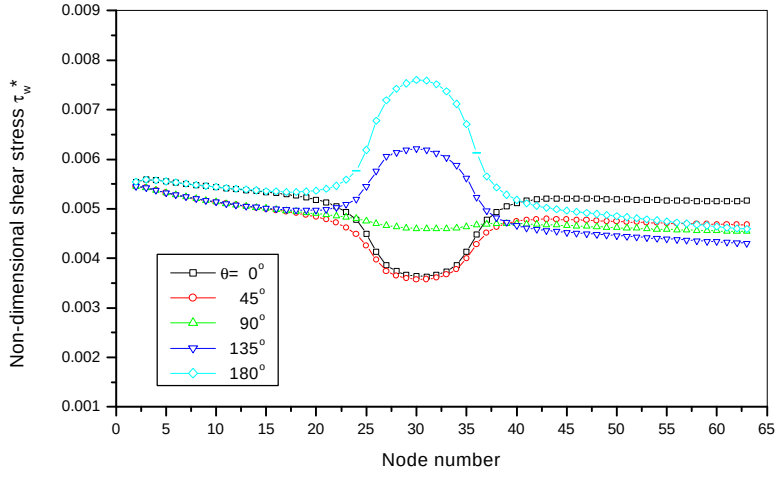

(c) α=150°

Fig. 7 Non-dimensional longitudinal shear stress distributions at the inner wall for the three curved pipes